Agora of Additive Manufacturing (2026) paper26001

JAMS

Agora of Additive Manufacturing

journal homepage: http://additive-manufacturing.or.jp/

Electrical Resistance Welding of 3D-Printed Short Carbon Fiber/PA-6 Using Laser Surface Treatment with Post-Smoothing

Masatoshi Enomoto[a], Akira Todoroki[b*]

a Graduate School of Engineering, Institute of Science Tokyo, Meguro, Tokyo, Japan

b Department of Mechanical Engineering, Institute of Science Tokyo, Meguro, Tokyo, Japan

ABSTRACT

The present study investigates resistance welding of 3D-printed short carbon fiber-reinforced thermoplastic (sCFRTP/PA-6) specimens using laser surface treatment combined with a novel smoothing post-treatment. The insulating sCFRTP surface is rendered conductive by laser irradiation, which locally exposes and accumulates carbon fibers. However, the resulting surface roughness (Sa = 16.7 μm, Sz = 257.6 μm) limits contact uniformity and welding area. To address this, a post-treatment clamping the laser-treated surface against a heated aluminum plate (180°C, 600 s, with release agent) was developed, reducing Sa to 3.1 μm and Sz to 43.6 μm while preserving electrical conductivity. Tensile shear tests demonstrated that the post-treatment significantly increased the true welding area and nominal joint strength. Under 2.0 MPa welding pressure, post-treated specimens achieved 3.70 MPa nominal strength—exceeding epoxy adhesive bonding (1.37 MPa)—with total process time of approximately 40 minutes versus 24 hours for adhesive curing.

Keywords: Resistance welding, 3D printing, short carbon fiber, thermoplastic composite, laser surface treatment, post-treatment

1. Introduction

Carbon fiber reinforced plastics (CFRP) are increasingly being adopted in the aerospace and automotive sectors as lightweight materials offering high strength and high stiffness (1)-(3). Recently, 3D printing has made it possible to fabricate carbon fiber reinforced thermoplastics (CFRTP), which have attracted attention for enabling high-mix low-volume production, automated manufacturing, and low-cost fabrication (4)-(8). Products 3D-printed by fused filament fabrication (FFF) are well suited to forming parts with complex geometries, but manufacturing large components remains difficult. They also suffer from low strength in the stacking direction (9). Todoroki et al. (10) proposed a method for reinforcing the stacking direction in which holes are created during 3D printing and continuous-fiber CFRTP is inserted into these holes and fusion-bonded. While this method is effective for thick-plate structures, it is unsuitable for thin-plate structures. For thin-plate structures, large structures can instead be realized by joining multiple 3D-printed parts.

The short carbon fiber reinforced thermoplastic (sCFRTP) filament used in FFF 3D printers is applied to the outer wall layers of composite prints to improve surface appearance and dimensional accuracy. This wall-forming sCFRTP filament must keep the fiber volume fraction as low as about 10% to maintain high dimensional accuracy and to prevent nozzle clogging. Owing to this manufacturing constraint, the CFRTP surface of a 3D-printed structure is currently an electrically insulating material.

Common joining methods for CFRTP are broadly classified into adhesive bonding, mechanical fastening, and fusion bonding (11). Adhesive bonding can achieve high strength with a suitable adhesive, but ensuring reliability is problematic

* Corresponding author
Email: todoroki.a.aa@m.titech.ac.jp
Received 17 April 2026; Revised 31 May 2026; Accepted 30 July 2026
Available online 5 August 2026

because nondestructive inspection of weak bonds is difficult [12],[13]. Metal bolt fastening provides stable joint strength, yet it causes delamination from bolt-hole machining [14],[15] and crushing due to compressive stress concentration [16]. It also adds weight because of the metal bolts.

Fusion bonding comprises three types: resistance welding, induction welding, and ultrasonic welding. Resistance welding melts the resin using Joule heat from an electrical resistance element placed between the parts [17], but the residual element has been noted to cause shear stress concentration and reduced corrosion resistance [18]. Induction welding heats the surface with eddy currents generated by an induction coil, but forming a uniform magnetic field is difficult, so the weld surface is heated nonuniformly [19]. Ultrasonic welding bonds parts through heat generated by ultrasonic vibration, but the welded region is limited to the area directly beneath the ultrasonic probe.

Enomoto and Todoroki proposed a novel resistance welding method for 3D-printed composite plates that use non-conductive sCFRTP filament in the wall, in which only part of the sCFRTP wall surface is selectively rendered conductive [20]. In this method, the insulating sCFRTP surface is laser-treated to locally ablate the surface resin, exposing and accumulating carbon fibers so that the surface fiber volume fraction rises locally and conductivity develops. A direct current is then applied to the conductive surface, and the resin is melted by Joule heat to weld the parts. This approach leaves no resistance element or other residue between the parts, and the welded region is not restricted to a spot. Enomoto and Todoroki [20] showed that conductivity develops under a defocused condition (60 mm distance) at a laser power of 40% and a travel speed of 5 mm/s, and that an application time of 15 s or more yields a joint strength (2.70–2.74 MPa) exceeding that of epoxy adhesive bonding (1.86 MPa). However, pronounced surface irregularities remained on the laser-treated surface, so that when two treated surfaces were brought into contact the contact was nonuniform; current therefore flowed only locally and the entire weld surface did not melt, which remained an issue.

Accordingly, this study aims to develop a post-treatment that reduces the surface roughness of the laser-treated surface (clamping against a heated aluminum plate) and to clarify how the presence or absence of this post-treatment and the applied pressure affect the weld area and joint strength. It also compares the processing time with that of adhesive bonding to demonstrate the practical advantage of the present welding method.

2. Experimental Methods and Preliminary Experimental Results

2.1 Materials, Specimens, and Preliminary Laser Treatment Experiment and Results

The specimens were fabricated using a Markforged Mark Two® 3D printer. The Mark Two® forms structures by the FFF process, melting and depositing sCFRTP (short-fiber CF/PA-6) at approximately 270 °C. The material used was Markforged sCFRTP filament Onyx® (fiber volume fraction 12.1%, mean fiber length 0.140 mm) (21). This Onyx® is an electrically insulating material (20). The specimen dimensions were 100 mm in length, 25 mm in width, and 4 mm in thickness, with 100% infill, ±45° orientation, a single-layer thickness of 0.125 mm, and 32 stacked layers (see Fig. 1).

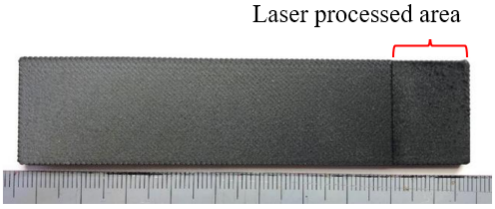

Fig.1 Specimen configuration.

In the previous report [20], the laser treatment conditions determined from a large number of trial settings (defocus distance 60 mm, laser power 40%, travel speed 5 mm/s) were adopted. The laser engraver used was an XTOOL D1Pro10W (wavelength 455 nm). At this wavelength of 455 nm, PA-6 transmits 80% of the laser light while the carbon fibers absorb it (22). Defocusing therefore heats the fibers over a wide area, scattering and burning off the resin (see Fig. 2). The treatment

area was 18.5 mm × 25 mm at the end of the specimen, of which 12.5 mm from the edge served as the weld region and the remaining 6 mm as the electrode formation region.

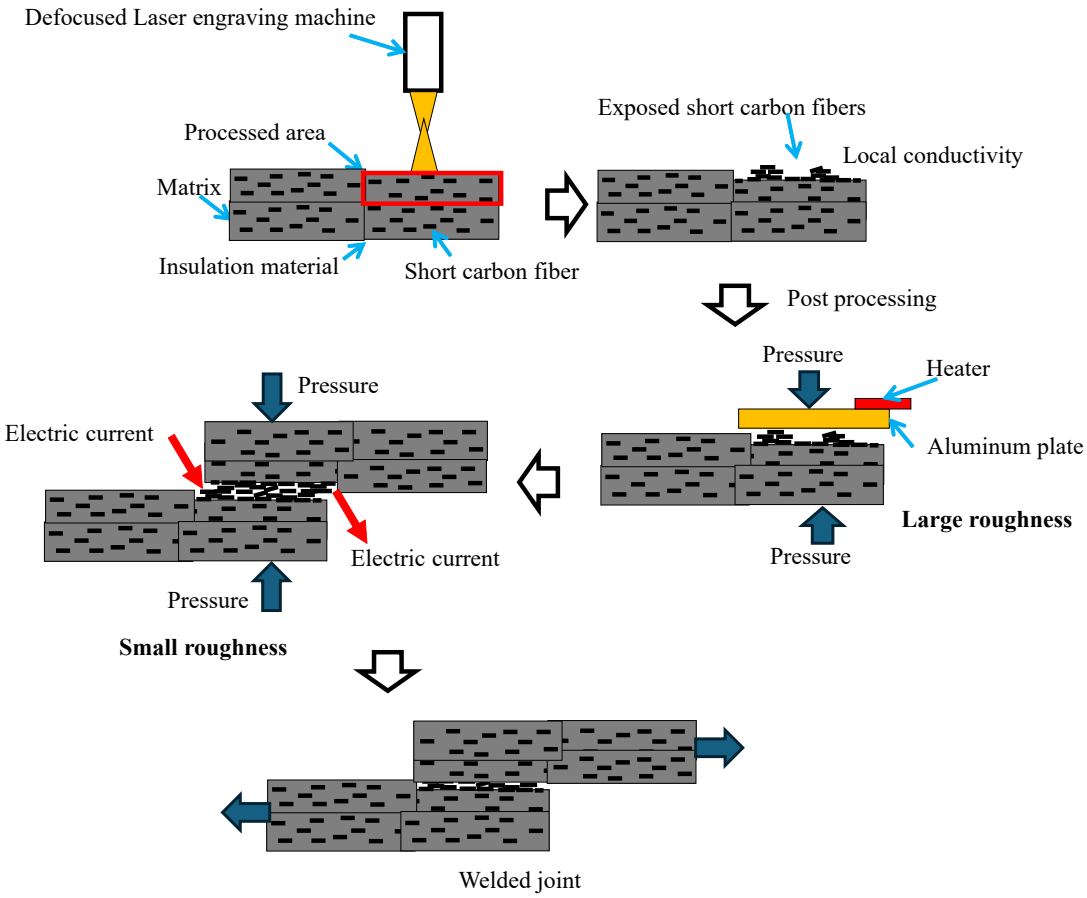

Fig2 Schematic representation of laser processing to make conductivity on surface of insulated sCFRTP.

2.2 Preliminary Experiment and Results for the Post-Treatment to Reduce Surface Irregularities

This laser treatment produces surface irregularities (arithmetic mean height S_a = 16.7 µm, maximum height S_z = 257.6 µm). To reduce these irregularities, this study applied a post-treatment in which the laser-treated surface was pressed against a heated aluminum plate and clamped. A cartridge heater was inserted into one end of the aluminum plate (lower part of Fig. 3, mean roughness S_a = 6.3 µm) and a thermocouple into the other end (upper part of Fig. 3), with the temperature regulated by a temperature controller. This is shown in Fig. 3.

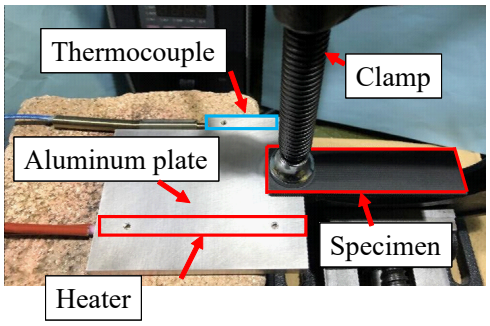

Fig.3 Experimental set up for post processing to reduce the roughness of surface.

As shown in the work by Cartledge and Baillie [23], the glass transition temperature of PA-6 is 50 °C and its melting point is 240 °C. To smooth the surface irregularities at elevated temperature, the specimen's irregular surface must be pressed against the flat aluminum plate and made to creep at a temperature above the glass transition temperature but below the melting point. In practice, a short processing time is desirable, but too high a temperature alters the shape of the molded part.

Therefore, as a preliminary experiment, the temperature and time were varied and the flattening conditions were set by visual inspection. The clamping torque was fixed at 1.0 N·m, corresponding to light tightening, based on the tightening torque used during welding in the previous report. Four conditions were first examined experimentally, combining two temperature settings (210, 240 °C) with two clamping times (10, 30 s). However, all of them produced large deformation of the specimen (see Fig. 4).

From this result, it was judged that the temperature was too high, so that even a mere 10 s of clamping caused substantial deformation. The temperature was therefore lowered to 150 °C and 180 °C and the clamping time extended to 600 s. Because the process is creep deformation, it was inferred that a lower temperature would lengthen the required time exponentially; the clamping time of 600 s was determined after observing the changes over several trials. As a result, the large deformation was eliminated, as shown in Fig. 5.

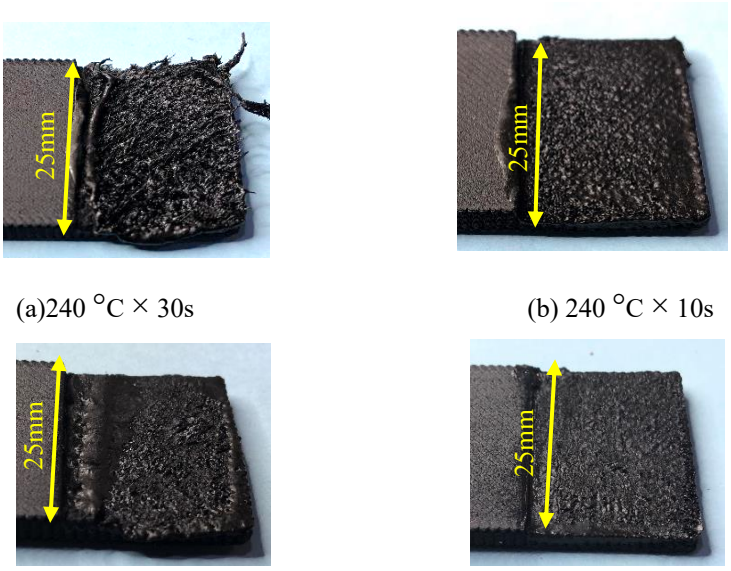

(a)240 °C × 30s (b) 240 °C × 10s

(c) 210 °C × 30s (d) 210 °C × 10s

Fig. 4 Results of preliminary examination under the conditions of 240 °C and 210 °C.

(a)180°C × 600s (b) 150°C × 600s

Fig. 5 Results of preliminary examination under the conditions of 180 °C and 150 °C.

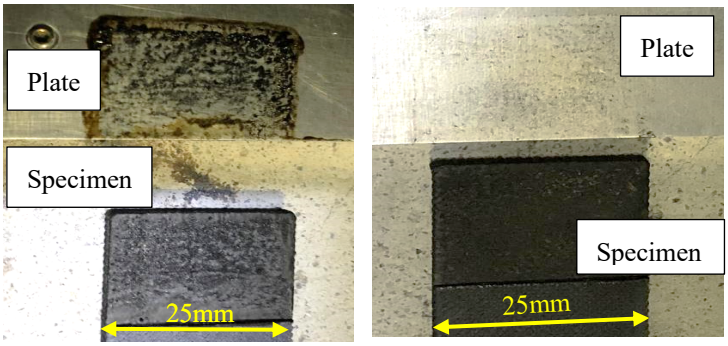

Fig. 6 Specimen and aluminum plate after clamping (left: heating temperature of aluminum plate is 180 °C, right: 150 °C).

However, at 180 °C the PA-6 was observed to adhere markedly to the aluminum plate (see Fig. 6). Resin adhesion to the aluminum plate indicates that irregularities arise from the peeling process that follows adhesion (see Fig. 6). Indeed, irregularities resembling those of the resin left on the aluminum plate were found on the specimen surface in Fig. 6. To avoid resin adhesion, an improvement was attempted by applying a release agent (LOCTITE FREKOTE 770-NC) to the aluminum plate. When the surface roughness was measured and compared at 150 °C and 180 °C, the large irregularities were eliminated at 180 °C, giving better roughness reduction. This is shown in Fig. 7.

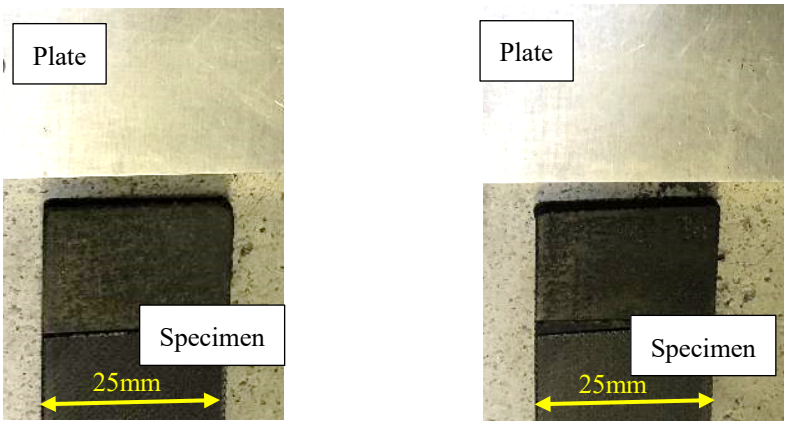

Fig. 7 Specimen and aluminum plate after clamping with release agent (left: heating temperature of aluminum plate is 180°C, right: 150°C).

The absence of release agent on the specimen was confirmed by FTIR measurement (Shimadzu IRAffinity-1). The ATR method was used, with 32 accumulations and a resolution of 4 cm^{-1}. FTIR measurements were performed on the specimen surface post-treated using an aluminum plate coated with release agent and on the specimen surface post-treated without release agent, and the spectra were compared. The release agent FREKOTE 770-NC consists of 80–100% naphtha and 1–5% of the reaction product of trimethylsilane and silanol-terminated polydimethylsiloxane. The FTIR results are shown in Fig. 8. The dashed line is the spectrum of the specimen surface post-treated with release agent applied, and the solid line is that of the specimen surface post-treated without release agent. Since the two spectra coincide, no difference in the surface composition of the specimen was observed with or without the application of release agent. This confirmed that no release agent adhered to the specimen surface post-treated with the release agent applied.

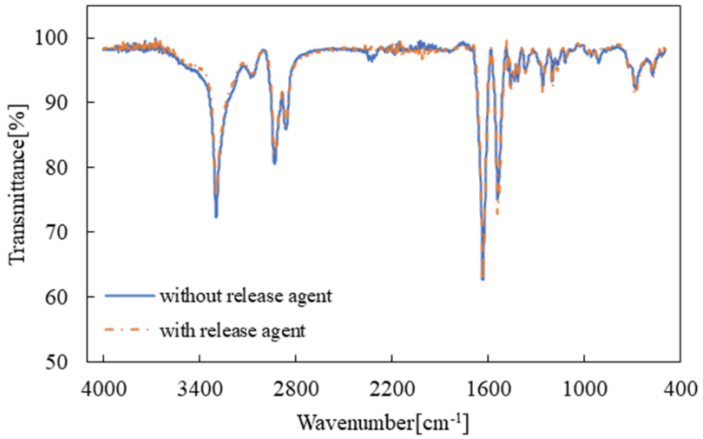

Fig.8 ATR-FTIR of specimen surfaces after post processing with/without release agent (preliminary experiments).

For comparison, the surface roughness was measured for laser treatment alone and for the post-treatment flattening process using two sets of process parameters: with release agent at 180 °C and without release agent at 150 °C. A non-contact one-shot 3D shape measuring instrument (Keyence VR-3100) was used, with a display resolution of 0.1 μm. The surface roughness was measured for the specimen post-treated under the conditions determined in the previous section (temperature 150 °C, clamping time 600 s) and for the laser-treated specimen. Because the instrument's specifications reduce measurement accuracy at low magnification, a magnification of 40× was selected, and the 7.6 mm × 5.7 mm area shown in Fig. 9 was measured. The region enclosed by the red frame in the figure is the surface roughness measurement area.

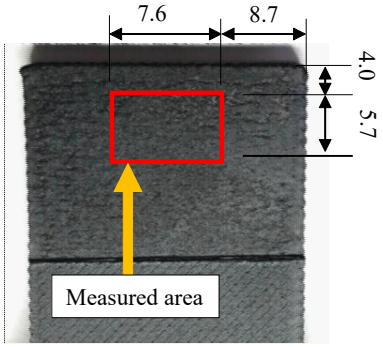

Fig.9 Measured area of the specimen for surface roughness (preliminary experiments).

First, the surface roughness of the laser-treated specimen was measured, after which the same specimen was post-treated and its surface roughness measured again. By measuring the same location on the same specimen, the change in surface roughness before and after post-treatment was evaluated. The averages for three specimens are shown in Table 1. For both the 180 °C and 150 °C treatments, the surface roughness after laser treatment was almost the same. In both cases the post-treatment reduced the surface roughness, but at 180 °C the mean value fell to about one-third of that at 150 °C, and the maximum height S_z at 180 °C fell to about half of that at 150 °C.

Table 1 Measured surface roughness (preliminary experiments).

	180 °C (with release agent)		150°C (without release agent)	
	Before	After	Before	After
S_a [μm]	15.6	3.1	16.7	9.0
S_z [μm]	259.9	43.6	257.6	96.2

Based on the above results, the process parameters for the post-treatment flattening were determined as follows: release agent applied, temperature 180 °C, clamping time 600 s, and tightening torque 1.0 N·m.

2.3 Preliminary Experiment and Results for Electrode Fabrication and Current Application

Two types of specimens were prepared—laser-treated Onyx specimens and specimens that were laser-treated and then post-treated—and welded by resistance heating with a direct current. For welding, flat plates 100 mm long, 25 mm wide, and 4 mm thick were 3D-printed, and single-lap joint specimens were made by welding a 12.5 mm end portion of two plates together. The laser-treated and post-treated surfaces are expected to exhibit anisotropy and variability in conductivity. Therefore, rather than attaching lead wires directly to the treated area to pass current, the lead wires were attached to electrodes, and current was passed from the electrodes to the treated area. One electrode was attached to each of the two Onyx® plates (see Fig. 10).

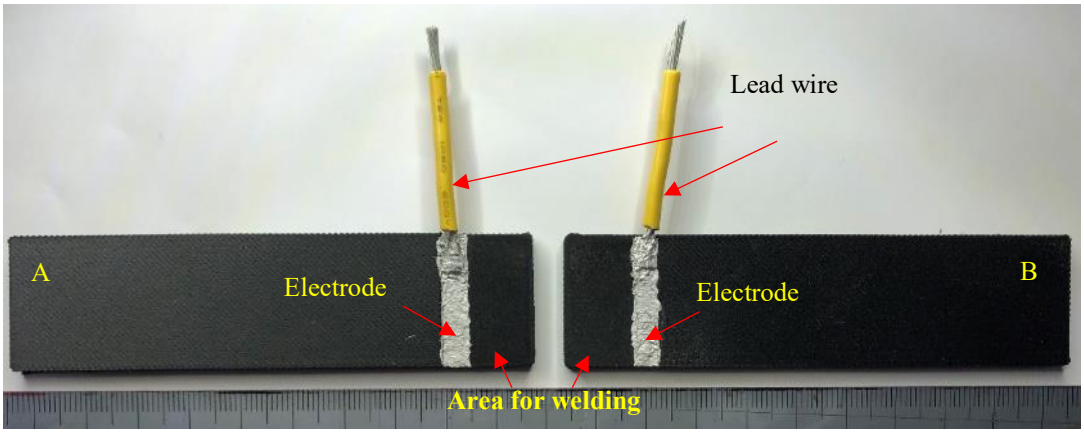

Fig. 10 Specimen for resistance welding (preliminary experiments).

For the specimen, the 18.5 mm end portion of a 3D-printed flat plate was laser-treated and post-treated; 12.5 mm from the edge was left as the weld portion, and the electrode was fabricated on the remaining 6 mm portion. To prevent detachment, the lead wire was temporarily fixed with epoxy adhesive (ThreeBond 2088E), after which silver paste (Dotite D-500) was applied to the lead wire end and to the electrode portion of the specimen to ensure conductivity. By bringing specimens A and B in Fig. 10 into contact with their treated surfaces facing each other, a current path running perpendicular to the interface was formed. However, unless the silver paste was applied all the way to the edge of the joint, a high-resistance region formed between the silver paste and the edge, causing the temperature there to rise intensively; therefore, after bringing specimens A and B into contact, additional silver paste was applied up to the edge as shown in Fig. 11.

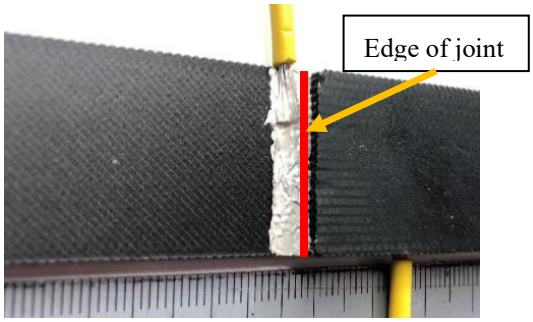

Fig. 11 Silver paste is painted at the edge of joint (preliminary experiments).

For pressurization during welding, two conditions of 0.8 MPa and 2.0 MPa were set within a range that would not damage the Onyx®, using a torque wrench, and the specimen was clamped in a vise. A plain-woven GFRP laminate was inserted between the vise and the Onyx® for insulation (see Fig. 12). A direct current was applied using a bipolar power supply (NF Corporation BP4620).

To determine an appropriate direct-current value, the side-surface temperature of the joint was measured with an infrared thermographic camera (FLIR ix, FLIR Systems), and a constant current was applied under several conditions. As a result, for laser treatment alone, the temperature and voltage rose sharply at 0.3 A after 38 s, confirming welding. The current for laser treatment alone was therefore set to 0.3 A. For the post-treated surface, a sharp rise in temperature and voltage and welding were confirmed at 1.1 A after 150 s. The current for the post-treated specimens was therefore set to 1.1 A.

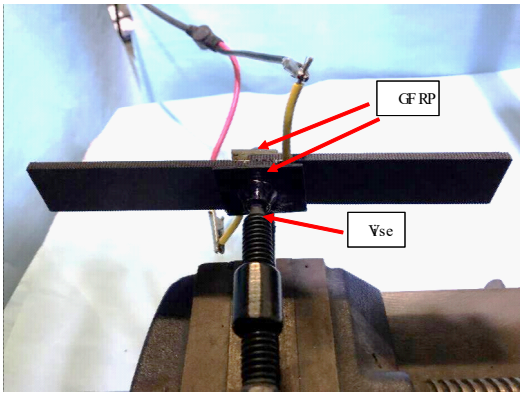

Fig.12 Experimental equipment for applying electric current.

2.4 Tensile Shear Test Method

After welding, plain-woven GFRP laminate tabs (25 mm long, 25 mm wide, 4 mm thick) were bonded to both ends of the single-lap joint with epoxy adhesive (3M DP420) (see Fig. 13). A Shimadzu universal testing machine (AG-I 100 kN) was used for the tensile shear test, with a test speed of 1.3 mm/min in reference to ASTM D1002. Five specimens were tested for each of the four welding conditions (laser treatment only / post-treatment, applied pressure 0.8 / 2.0 MPa).

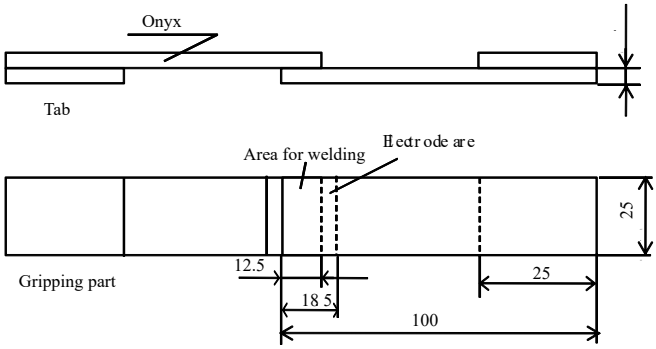

Fig.13 Tensile shear test specimen

For evaluating the joint strength, two measures were used: the joint strength based on nominal stress (nominal joint strength) s_n, given by Eq. (1), and the joint strength based on true stress (true joint strength) s_t, given by Eq. (2).

$$\sigma_n = \frac{P}{A_j} \quad (1)$$

$$\sigma_t = \frac{P}{A_w} \quad (2)$$

Here, A_j is the nominal joint area, taken as 12.5 mm × 25 mm = 312.5 mm². A_w is the true weld area, calculated from fracture surface observation after testing. P is the load. The true joint strength is an index of the inherent strength of the welded portion, whereas the nominal joint strength is an index of the strength of the joint as a whole. The maximum load was used in the strength calculations.

For comparison, a tensile shear test was conducted under the same conditions on adhesive-bonded specimens using epoxy adhesive (Araldite Rapid) (same dimensions, applied over a 12.5 mm end region, cured for 24 hours). The effects of the presence or absence of post-treatment and of the applied pressure were evaluated for statistical significance using a t-test (two-tailed, significance level $p < 0.05$).

3. Joint Strength Test Results and Discussion

The nominal stress–displacement relationships for laser treatment alone at applied pressures of 0.8 MPa and 2.0 MPa are shown in Fig. 14(a) and (b), respectively. The vertical axis is nominal stress and the horizontal axis is testing-machine displacement. The nominal stress–displacement relationships for the case where post-treatment was performed after laser treatment, at applied pressures of 0.8 MPa and 2.0 MPa, are shown in Fig. 15(a) and (b), respectively. For comparison, the nominal stress–displacement relationship for the adhesive-bonded case is shown in Fig. 16.

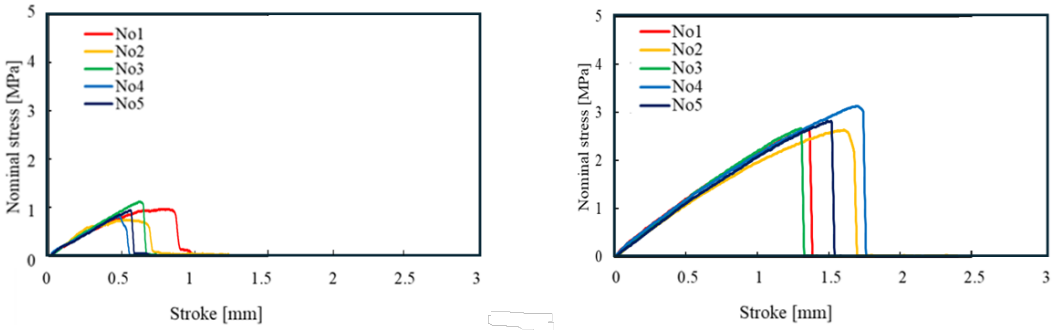

(a) welding pressure: 0.8 MPa (b) welding pressure: 2.0 MPa

Fig.14 Tensile shear test results of single-lap joints (laser processing only).

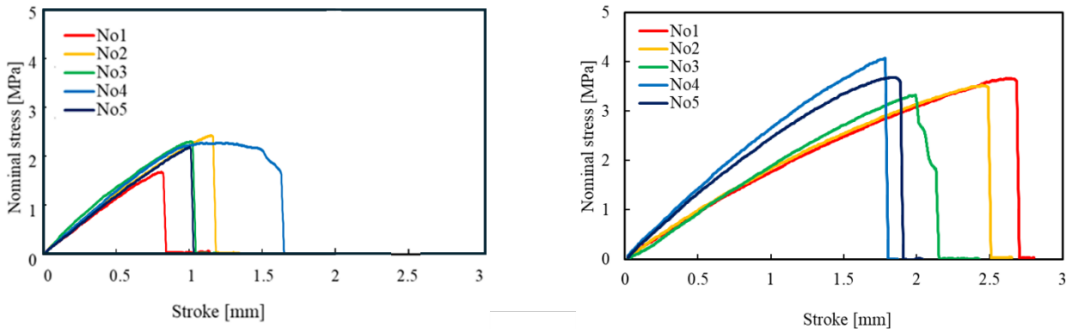

(a) welding pressure: 0.8 MPa (b) welding pressure: 2.0 MPa

Fig.15 Tensile shear test results of single-lap joints (with post processing).

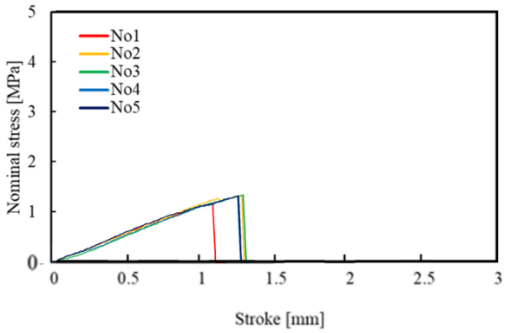

Fig.16 Tensile shear test results with adhesive bonding.

The true weld area A_w was determined from fracture surface observation after testing. Representative fracture surfaces are shown in Fig. 17 (0.8 MPa) and Fig. 18 (2.0 MPa). It can be seen that the post-treatment increased the weld area.

(a) Laser processing only (b) With post processing

Fig.17 Fracture surface of welded specimen after tensile shear test (0.8 MPa).

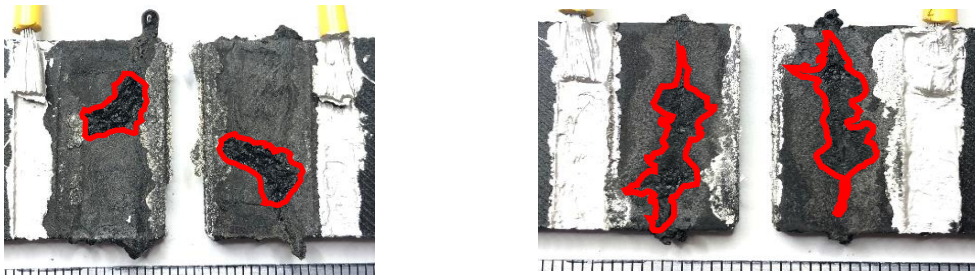

(a) Laser processing only (b) With post processing

Fig.18 Fracture surface of welded specimen after tensile shear test (2.0 MPa).

The mean values and standard deviations of the nominal joint strength, true joint strength, and weld area for the joints welded under each condition are shown in Table 2. The t-test results for the presence or absence of post-treatment are shown in Table 3, and those for the applied pressure in Table 4.

Table 2 Nominal joint strength, true joint strength and welding area of tensile shear test of single-lap joints.

Welding pressure [MPa]	Specimen surface	Nominal joint strength (STD) [MPa]	True joint strength (STD) [MPa]	Welding area (STD) [mm^2]
0.8	Post processing	2.22 (0.280)	11.4 (1.79)	61.4 (8.88)
	Laser processing	0.980 (0.124)	12.5 (1.17)	24.6 (2.80)
2.0	Post processing	3.70 (0.267)	14.4 (3.12)	82.5 (13.4)
	Laser processing	2.81 (0.214)	14.4 (1.54)	61.2 (2.98)

Table 3 The p-value of t-test conducted between post processing and laser processing.

Welding pressure [MPa]	Nominal joint strength (STD) [MPa]	True joint strength (STD) [MPa]	Welding area (STD) [mm^2]
0.8	1.6×10^{-4}	0.30	3.8×10^{-4}
2.0	4.9×10^{-4}	0.98	0.021

Table 0 The p-value of t-test conducted between 0.8MPa and 2.0MPa.

Specimen surface	Nominal joint strength (STD) [MPa]	True joint strength (STD) [MPa]	Welding area (STD) [mm^2]
Post processing	2.8×10^{-5}	0.11	0.021
Laser processing	1.6×10^{-6}	0.058	4.2×10^{-8}

In Fig. 18, the silver paste on the edge portion, as shown in Fig. 11, is that which was additionally applied to the edge after combining specimens A and B and then soaked in. In general, the room-temperature cured strength of an acrylic conductive adhesive is negligibly small compared with the strength of PA-6 [24]; therefore, the portion into which the silver paste soaked is not taken into account here.

At an applied pressure of 0.8 MPa, post-treatment increased the true weld area by about 2.5 times and the nominal joint strength by about 2.3 times compared with laser treatment alone. At an applied pressure of 2.0 MPa as well, post-treatment increased the true weld area by about 1.3 times and the nominal joint strength by about 1.3 times. This is considered to be because the reduction in surface roughness by post-treatment increased the contact area, thereby improving the true weld area and the nominal joint strength. Under both applied-pressure conditions, significant differences were found in the true weld area and the nominal joint strength (Table 3). For the true joint strength, no significant difference was found with or without post-treatment ($p > 0.05$), showing that the local strength of the welded portion is equivalent regardless of post-treatment.

Comparing the applied pressures for the post-treated joints, at 2.0 MPa the true weld area increased by about 1.3 times and the nominal joint strength by about 1.7 times compared with 0.8 MPa. For laser treatment alone as well, at 2.0 MPa the true weld area increased by about 2.5 times and the nominal joint strength by about 2.9 times compared with 0.8 MPa. This is considered to be because the increase in applied pressure reduced the gaps at the weld interface and thereby enlarged the contact area. Significant differences were also found in the true weld area and the nominal joint strength for the effect of applied pressure.

The nominal stress of the epoxy adhesive bond was 1.37 MPa. With the present welding method, a strength of 3.70 MPa was obtained under the post-treatment, 2.0 MPa applied-pressure condition, substantially exceeding that of adhesive bonding. In terms of the time required for joining, whereas epoxy adhesive bonding requires 24 hours of curing time, the present welding method completes joining in a total of about 40 minutes: 27 minutes of laser treatment, 10 minutes of post-treatment, and about 3 minutes of current application.

4. Conclusions

In this study, for the electrical resistance welding method using laser surface treatment of 3D-printed insulating sCFRTP proposed in the previous report, the effect of a post-treatment (clamping against a heated aluminum plate) in reducing surface roughness, and the influence of the presence or absence of post-treatment and of the applied pressure on joint strength, were experimentally verified. The conclusions obtained are as follows.

(1) The post-treatment (600 s) of clamping the laser-treated surface against a release-agent-coated aluminum plate at 180 °C reduced the arithmetic mean height Sa from 16.7 μm to 3.1 μm and the maximum height Sz from 257.6 μm to 43.6 μm, and the surface conductivity was confirmed to be maintained.

(2) The post-treatment significantly increased the true weld area and the nominal joint strength; under the 0.8 MPa applied-pressure condition, the nominal stress became 2.3 times and the true weld area 2.5 times greater. There was no significant difference in the true joint strength, indicating that the post-treatment improves joint strength through enlargement of the weld area.
(3) An increase in applied pressure produced a statistically significant increase in the true weld area and the nominal joint strength. Under the post-treatment and 2.0 MPa applied-pressure condition, a nominal joint strength of 3.70 MPa and a weld area of 82.5 mm² were obtained.
(4) The present welding method can achieve a joint strength exceeding that of adhesive bonding (1.37 MPa, 24-hour curing) in about 40 minutes, confirming its advantage also in terms of joining efficiency.

Acknowledgments
This work was supported by a Grant-in-Aid for Scientific Research (C) (General) (24K08053) from the Japan Society for the Promotion of Science.

References
(1) Kaufmann M, Zenkert D and Wennhage P. Integrated cost/weight optimization of aircraft structures, Structural and Multidisciplinary Optimization, 2009;41(2);325-334.
(2) Roeseler WG, Sarh B, Kismarton MU. Composite structures: the first 100 years. 16th International Conference on Composite Materials (ICCM-16), Kyoto, Japan. https://doi.org/10.5281/zenodo.15414625.
(3) https://www.boeing.com/commercial/787/by-design/#/advanced-composite-use. (Accessed April 16, 2026)
(4) Ning F, Cong W, Qiu J, Wei J, Wang S. Additive manufacturing of carbon fiber reinforced thermoplastic composites using fused deposition modeling, Compos. Part B: Engineering, 2015;80;369-378.
(5) Matsuzaki R, Ueda M, Namiki M, Jeong TK, Asahara H, Horiguchi K, Nakamura T, Todoroki A, Hirano Y. Three-dimensional printing of continuous-fiber composites by in-nozzle impregnation, Scientific reports, 2016;6(1); #23058.
(6) Li N, Li Y, Liu S. Rapid prototyping of continuous carbon fiber reinforced polylactic acid composites by 3D printing, Journal of Materials Processing Technology, 2016;238;218-225.
(7) Lewicki JP, Rodriguez JN, Zhu C, Worsley MA, Wu AS, Kanarska Y, Horn JD, Duoss EB, Ortega JM, Elmer W, Hensleigh R, Fellini RA, King MJ. 3D-printing of meso-structurally ordered carbon fiber/polymer composites with unprecedented orthotropic physical properties, Scientific Report, 2017; 7 (1); #43401.
(8) Liu T, Tian X, Zhang M, Abliz D, Li D, Ziegmann G. Interfacial performance and fracture patterns of 3D printed continuous carbon fiber with sizing reinforced PA6 composites, Composites Part A, Applied Science and Manufacturing, 2018;114;368–376.
(9) Todoroki A, Oasada T, Mizutani Y, Suzuki Y, Ueda M, Matsuzaki R, Hirano Y. Tensile Property Evaluations of 3D Printed Continuous Carbon Fiber Reinforced Thermoplastic Composites, Advanced Composite Materials, 2020;29(2); 147-162.
(10) Todoroki A, Oasada T, Ueda M, Matsuzaki R, Hirano Y. Reinforcing in the lay-up direction with self-heating for carbon fiber composites fabricated using a fused filament fabrication 3D printer, Composite Structures, 2021;266; #113815.
(11) Pramanik A, Basak AK, Dong Y, Sarker PK, Uddin MS, Littlefair G, Dixit AR, Chattopadhyaya. Joining of carbon fibre reinforced polymer (CFRP) composites and aluminium alloys - A review, Composites Part A: Applied Science and Manufacturing, 2017;101;1-29.
(12) Haghani R. Analysis of adhesive joints used to bond FRP laminates to steel members - A numerical and experimental study, Construction and Building Materials, 2010;24(11);2243-2251.
(13) Drewry MA, Smith RA, Phang A, Yan D. Ultrasonic Techniques for Detection of Weak Adhesion, Materials Evaluation, 2009;67(9);1048-1058.

(14) Prakash M, Pallapothu H, Laxminarayana P. A Review on Micro Drilling of Glass Fiber Reinforced Polymer Composites, International Journal for Research in Applied Science and Engineering Technology, 2019;7(5);3612-3615.
(15) Shyha IS, Aspinwall DK, Soo SL, Bradley S. Drill geometry and operating effects when cutting small diameter holes in CFRP, International Journal of Machine Tools and Manufacture, 2009;49(12-13);1008-1014.
(16) Xiao Y, Ishikawa T. Bearing strength and failure behavior of bolted composite joints (part I: Experimental investigation), Composites Science and Technology, 2005;65(7–8);1022-1031.
(17) Stavrov D, Bersee HEN. Resistance welding of thermoplastic composites-an overview, Composites Part A Applied Science and Manufacturing, 2005;36(1);39-54.
(18) Todd SM. Joining thermoplastic composite, Proceedings of the 22nd International SAMPE Technical Conference, 1990;22;383-392.
(19) Ahmed J, Stavrov D, Bersee HEN, Beukers A. Induction welding of thermoplastic composites-an overview", Composites Part A Applied Science and Manufacturing, 2006;37(10);1638-1651.
(20) Masatoshi Enomoto, Akira Todoroki, Electric resistance welding of 3D printed short carbon fiber/PA-6 using Laser surface treatment , Reinforced Plastics, 2024;70(6); 202-207. (in Japanese)
(21) Yoichiro Koga, Akira Todoroki, Yoshihiro Mizutani, Yoshiro Suzuki. Deflection of deposited short fiber and anisotropic mechanical properties of 3D printed isotropic short fiber reinforced plastics based on Fused Deposition Molding, Reinforced Plastics, 2017; 63(12);604-608. (in Japanese)
(22) Fischer F, Romoli L, Kling R. Laser-based repair of carbon fiber reinforced plastics, CIRP Annals, 2010;59(1), 203-206.
(23) Helen C. Y. Cartledge & Caroline A. Baillie, Studies of microstructural and mechanical properties of nylon/glass composite Part I The effect of thermal processing on crystallinity, transcrystallinity and crystal phases, Journal of Materials Science, 1999;34;5099-5111.
(24) https://pub-mediabox-storage.rxweb-prd.com/exhibitor/document/exh-ba3595ec-5620-4c6f-9fc0-144418a0adad/81f22bb7-a0c1-48c0-ba73-4d4062372a74.pdf (Accessed May 31, 2026)